Tectonophysics 877 (2024) 230284

Contents lists available at ScienceDirect

Tectonophysics

journal homepage: www.elsevier.com/locate/tecto

A large fault partially reactivated during two contiguous seismic sequences in Central Italy: The role of geometrical and frictional heterogeneities

M.E. Locchi [a,*], L. Scognamiglio [b], E. Tinti [a,b], C. Collettini [a]

[a] Department of Earth Sciences, La Sapienza University of Rome, Italy
[b] Istituto Nazionale di Geofisica e Vulcanologia, Rome, Italy

ARTICLE INFO

Keywords:
Moment tensor
Seismicity
Slip-tendendy
Normal fault
Coseismic-slip
Friction

ABSTRACT

Earthquakes can rupture multiple fault segments as well as faults with complex geometry, or heterogeneous pre-stress and frictional properties. These observations have been documented mainly for moderate-to-large earthquakes by inverting geodetic and seismic data and by studying the influence of fault orientation and rheology within the regional stress field.

In this work we have studied the Gorzano fault, GF, a large normal fault within the active fault system of Central Italy that during the last two largest Italian seismic sequences, L'Aquila (2009) and Amatrice-Visso-Norcia (2016–2017), was reactivated via a series of $5.0 < Mw < 6.0$ events. We calculated moment tensor solutions for 134 $M > 3$ events and evaluated their normalized slip-tendency. Merging these results with high resolution earthquake catalogs, available $M > 5$ earthquake slip distributions, and frictional properties characterizing the activated fault, we develop a mechanical model and discuss potential earthquake rupture scenarios.

The GF is an optimally oriented fault within the regional stress field and from, the reactivation via aftershock or mainshock slip of complementary fault portions from 2009 to 2017 indicates that the fault behaves as a single fault structure. The geometrical and mechanical heterogeneities suggest that the most likely slip behavior of GF is the reactivation of different fault portions with $M > 5.0$. However, due to favorable initial stress conditions, we suggest that a seismic rupture can produce the complete reactivation of the fault, resulting in a M 6.5–6.6 earthquake as documented in paleoseismological data.

1. Introduction

Several factors influence the possibility that one seismic event ruptures through small portions or the entire fault length and/or jumps from one fault segment to another. The primary control on final rupture length and therefore on the arrest of the rupture is mainly exerted by the stress state, fault frictional properties, and by the geometry of the fault system.

Fault segments or fault portions more prone for earthquake nucleation are those critically stressed within the regional stress field (Walsh and Zoback, 2016). Once initiated, an earthquake rupture can activate small portions or the entire fault plane or even can jump on adjacent fault segments more easily if the stress level approaches that of failure (Scholz, 2010; Tinti et al., 2021) and/or when the degree of stress interaction between faults is high (Scholz and Gupta, 2000).

Geometrical complexities such as fault steps (Biasi and Wesnousky, 2016) or dilational jogs (Sibson, 1985) seem to play an important role for earthquake rupture stopping. Field observations on a large number of surface ruptures indicate that fault step-over larger than 4–5 km are very efficient to stop fault rupture propagation, with dip-slip ruptures capable of crossing larger steps than strike-slip earthquakes (Biasi and Wesnousky, 2016). In areas characterized by tectonic inversion, inherited fault structures can work as either structural barriers for rupture propagation (Collettini et al., 2005; Pizzi and Galadini, 2009) or as sites for stress concentrations where the seismic rupture can nucleate or easily pass through (Pizzi et al., 2017; Scognamiglio et al., 2018).

Spatial variation of fault frictional properties is another determining factor for earthquake rupture size (Kaneko et al., 2010; Barbot, 2021). Numerical models coupled with geodetic and seismic observations indicate that earthquake rupture patterns are strongly connected with spatial variation of friction. Earthquake propagation through a rupture-impeding, rate strengthening patch, is generally difficult (Kaneko et al., 2010; Thomas et al., 2014, Barbot, 2019, among many others). However, for some events, like the 2011 Tohoku-Oki Mw = 9.0 earthquake,

* Corresponding author.
E-mail address: mariaeugenia.locchi@uniroma1.it (M.E. Locchi).

https://doi.org/10.1016/j.tecto.2024.230284
Received 19 July 2023; Received in revised form 13 March 2024; Accepted 19 March 2024
Available online 21 March 2024

coseismic weakening promoted by rapid shear heating of pore fluids allowed earthquake slip to occur within a fault portion characterized by rate strengthening friction (Faulkner et al., 2011; Noda and Lapusta, 2013).

Some recent case studies of large earthquakes provided important observations indicating that seismic ruptures in the same area may differ significantly in extent and magnitude and that rupture jumps can be very efficient and sometimes difficult to be predicted. Examples have been documented in Sumatra megathrust (Konca et al., 2008), in the 2023 south-central Turkey earthquake (Dal Zilio and Ampuero, 2023) and in the 2016 Kaikoura earthquake in New Zealand (Hamling et al., 2017). These examples of multiple and complex ruptures during large earthquakes pose some doubts on how efficient fault segmentation, variable fault geometry and fault step-over are in stopping earthquakes. In this work we contribute to this topic by presenting an example of a fault that in eight years was almost entirely reactivated by a series of $5 < M < 6$ earthquakes without experiencing any full rupture. In the discussion we analyze the fault geometrical and frictional heterogeneities to discuss possible earthquake rupture behavior.

2. Seismotectonic setting and the Gorzano fault

The study area is located in the Central Apennines, an area affected by a Late Miocene-Early Pliocene compressional phase producing N-S trending east-verging anticlines and west-dipping thrust faults. This compressional phase was followed by Late Pliocene–Quaternary extension accommodated along NW-SE trending normal faults (Lavecchia et al., 1994; Pizzi and Galadini, 2009; Barchi et al., 2021). Active extension is occurring at rates of about 3 mm yr^{-1} (Serpelloni et al., 2005; Anderlini et al., 2016), promoting several major seismic sequences in the last 25 years: Colfiorito 1997, CO, Mw = 6.0 (Chiaraluce et al., 2003), L'Aquila, AQ, 2009 Mw = 6.1 (Chiarabba et al., 2009), Amatrice-Visso-Norcia, AVN, 2016–2017 Mw = 6.5 (Chiaraluce et al., 2017). These sequences occurred along NW-trending and SW-dipping normal faults that bound the intermountain basins of the area.

In this work we studied the Gorzano normal fault (Boncio et al., 2004a, 2004b; Valoroso et al., 2013; Chiaraluce et al., 2017; Falcucci et al., 2018; Cheloni et al., 2019; Michele et al., 2020; Barchi et al., 2021; Buttinelli et al., 2021) located in the overlap zone between the SSE termination of the AVN sequence and the NNW portion of the AQ sequence (Fig. 1).

Among the many faults in the Central Apennines, the Gorzano fault (GF) is one of the most discussed and debated in the literature. Building on the interpretation of seismic reflection profiles (Bigi et al., 2011; Buttinelli et al., 2021) the fault mapped at the surface is considered detached from its deeper portion by an early Pliocene thrust and passively transported on its hanging-wall. In this interpretation the seismicity recorded during AQ 2009 and AVN 2016 sequences is occurring along an inherited normal fault located in the footwall of the thrust that is not connected with the mapped GF at the surface (Buttinelli et al., 2021). In marked contrast, a continuity of the GF from the surface into the seismogenic layer (as a single structure) is proposed by the integration of structural and morphotectonic features with three small magnitude seismic sequences M < 4, occurred in the area between 1992 and 1996 (Boncio et al., 2004a, 2004b). This interpretation is consistent with geomorphological analyses coupled with seismological and geodetic data related to the AQ 2009 and AVN 2016 sequences (Falcucci et al., 2018), with a different seismic reflection profiles interpretation (Barchi et al., 2021) and supported by paleoseismological studies documenting a maximum magnitude of ~6.6 for the GF (Galadini and Galli, 2003). Within the literature supporting the continuity of GF from shallow crustal levels down to seismogenic depths, some differences are present. For example, a single fault about 28 km long has been proposed in Boncio et al., 2004a or Lavecchia et al., 2012, whereas a two aligned but kinematically independent faults, the minor Amatrice fault and the major Campotosto fault has been identified in Galadini and Galli, 2003 and Falcucci et al., 2018.

In this paper we will present further data supporting the existence of

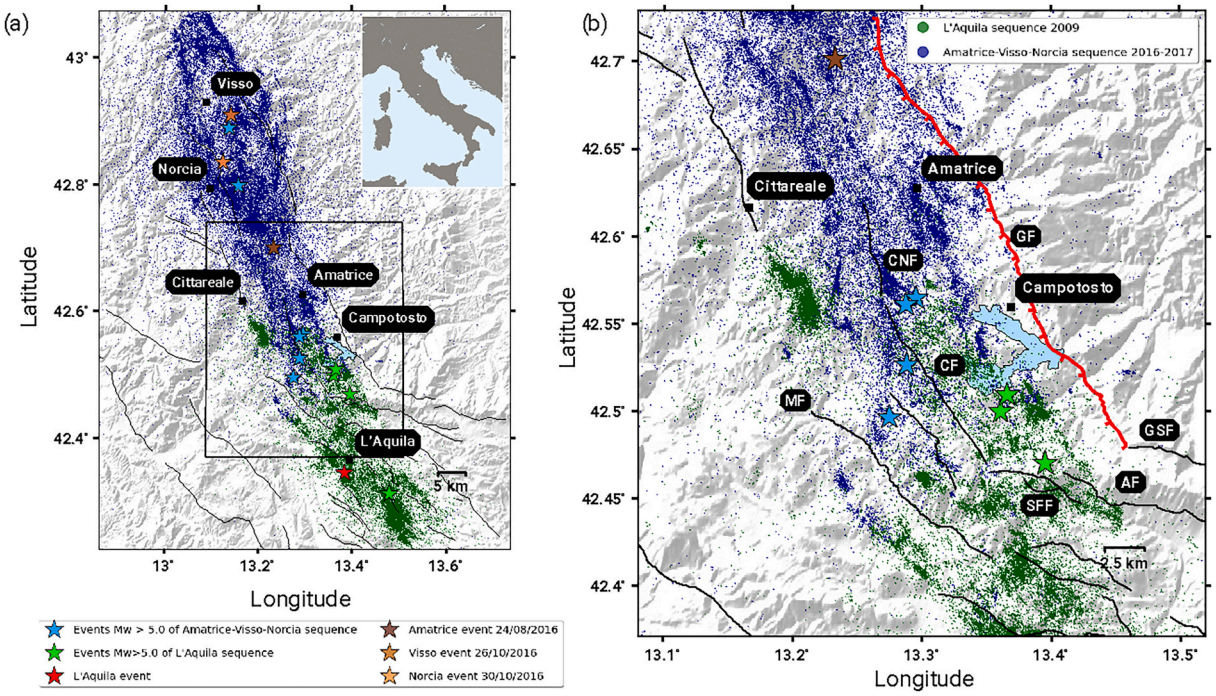

Fig. 1. (a). Map of the Amatrice-Visso-Norcia (AVN) and L'Aquila (AQ) seismic sequences colour-coded by seismic catalog: Waldhauser et al., 2021 (dark blue) and Valoroso et al., 2013 (dark green). Light blue stars are events with Mw >5.0 of AVN sequence (2016–2017); light green stars are events with Mw >5.0 of AQ sequence (2009); brown stars are the mainshocks of AVN sequence: Amatrice Mw 6.0, Visso Mw 5.9 and Norcia Mw 6.5; red star is the L'Aquila Mw 6.0 mainshock. The black box frames the study aea zoomed in panel (b). (b). Black lines are the traces of the main normal faults (Villani et al., 2018): GF = Gorzano fault (red solid line); CF = Capitignano fault; GSF = Gran Sasso fault; MF = Montereale fault; SFF = Mt. San Franco fault; AF = Assergi fault; CNF = Configno fault.

a continuous fault or fault system from the surface to the seismogenic depth leading us to consider this as the most likely interpretation for the GF. In addition, we will discuss how geometrical and frictional heterogeneities may influence earthquake rupture behavior and their effect on the conditions required to have partial or full ruptures.

3. Data & methods

3.1. Seismicity

Thanks to a dense network of seismic stations deployed during the AQ and AVN seismic sequence, many aftershocks were collected and resulted in high-resolution catalogs that can be used to describe the time-space evolution of the activity of the Gorzano fault. In this paper we use the seismicity distribution, from Valoroso et al., 2013 and Waldhauser et al., 2021 catalogs, to reconstruct the geometry of activated structure and to investigate the geometrical and temporal continuity of the two main sequences that affected the Gorzano fault.

The catalog adopted for the 2009 AQ sequence (Valoroso et al., 2013) is composed of 64,051 events (dark green dots in Fig. 1a) located by using an automatic P and S wave picking procedure together with cross-correlation and the double-difference (DD) HypoDD method (Waldhauser et al., 2021). The median error values derived from the bootstrap distribution are: 0.024 km along the major horizontal, 0.015 and 0.027 km along the minor horizontal and vertical directions, respectively. The events of this catalog located on the Gorzano fault area (Fig. 1b) and used in the following analyses are 32,000. For the AVN sequence (2016–2017) we use the seismic catalog of Waldhauser et al., 2021 with nearly 400,000 aftershocks (dark blue dots in Fig. 1a) obtained from automatically revised P and S picking (Spallarossa et al., 2021) and located with HypoDD. In Waldhauser et al. (2021), the median horizontal and vertical errors are 0.048 and 0.077 km, respectively. The events of this catalog located within the Gorzano fault area (Fig. 1b) and used in this paper are 116,000.

3.2. Moment tensor solutions

A detailed analysis on the kinematics of the Gorzano fault has been performed by building a new moment tensor catalog of the Campotosto area by applying the Time Domain Moment Tensor technique (hereafter TDMT) originally proposed by Dreger and Helmberger (1993) and Pasyanos et al. (1996) and successively implemented at INGV by Scognamiglio et al. (2009). To do that, we reviewed and improved 80 already published moment tensor solutions by increasing the number of inverted stations and computed 52 new solutions that lower the minimum magnitude threshold to M=3.0 having in total 134 available solutions for the Campotosto area from January 2009 until January 2021.

These solutions providing the strike, dip, and rake of the two possible conjugate fault planes, allow us to constrain the geometry and kinematics of small structures, and compare their consistency with the regional stress field. The TDMT solutions are computed by changing the centroid location within a 5 km wide interval around the hypocenter depth with a 1 km step, and ultimately selecting the best solution. Through TDMT we can estimate the moment magnitude (Mw) and evaluate the percentage of double couple (DC) and compensated linear vector dipole (CLVD), while the isotropic component (ISO) is constrained to be zero. The double-couple (DC) represents the force equivalent of a shear faulting mechanism on a planar fault; however, many moment tensor solutions reveal that seismic sources often display significant non-double-couple components: ISO (isotropic) and CLVD (compensated linear vector dipole). The ISO component accounts for a change in the volume, as in implosion or explosion events (e.g. nuclear explosions or induced seismicity) and it could be significant in volcanic earthquakes. The CLVD component represents a type of volumetric deformation, where rocks undergo both compaction and dilatation during an earthquake. It is often associated with earthquakes occurring in more complex geological regions, such as volcanic systems or regions with significant tectonic stress variations or it could represent a complex earthquake source mechanism, like a variability in fault geometry. A low CLVD value is usually related to uncertainties in the adopted Green functions or potential errors in the recorded data. The moment tensor solution is determined by fitting the synthetic seismograms to the observed data in a frequency range of 0.02–0.05 Hz or 0.02–0.1 Hz for events with Ml≥4 or Ml < 4, respectively. Its quality is measured through the variance reduction (VR) parameter, i.e., a misfit function between recorded and synthetic waveforms (Eq. 1):

$$VR = \sum_i w_i \left(1 - \frac{\int [x_i(t) - d_i(t)]^2 \, dt}{\int d_i^2(t) \, dt}\right) 100\% \quad (1)$$

where i is the station index, $x_i(t)$ is the synthetic waveform, $d_i(t)$ is the recorded waveform, and w_i is a weight proportional to the epicentral distance. In the context of Central Italy, the best solutions are those with a high DC percentage (>80%), VR > 50%, and the number of stations inverted >4. These parameters refer to the MT Quality Index used at INGV to assign a quality value to solutions and publish them on the website based on this index (see Fig. 3 of Scognamiglio et al., 2009).

Together with seismicity distribution and moment tensor solutions, to further analyze the geometry and slip of the activated fault system, we also reported along the Gorzano Fault the coseismic slip and post-seismic slip modeled for Mw > 5.0 during the 2009 AQ sequence (Cheloni et al., 2014), the two main events of January 2017 Mw 5.5 and 5.4 (Cheloni et al., 2019), and the coseismic slip of the Mw 6.0 Amatrice event (Tinti et al., 2016). It is worth emphasizing that the Amatrice Mw 6.0 mainshock produced fault reactivation in both the GF fault and Mt. Vettore fault (Tinti et al., 2016; Pizzi et al., 2017; Gallovič et al., 2019). The earthquake nucleated on the northernmost portion of GF releasing a first main slip patch up-dip from the hypocenter and then propagated northwards onto the southern Vettore fault releasing a second extended slip patch (Fig. S2). The equivalent Mw released by the slip patch belonging to the Gorzano fault is ~ 5.8 while most of the dislocation occurred in the southern part of the adjacent Mt. Vettore fault released an equivalent Mw ~ 5.95 (the total moment magnitude retrieved for the extended source model by inverting strong motion data is 6.1 similar to the TDMT solution Mw = 6.0).

3.3. Slip tendency

The potential of fault reactivation within a regional stress field can be assessed using a slip-tendency analysis. In this analysis the Amontons' law ($\tau = \mu \sigma n$) is used to evaluate the condition to slip on a fault, as:

$$Ts = \tau/\sigma_n \geq \mu_s \quad (2)$$

where τ and σ_n are the shear and effective normal stress on the fault, respectively, μ_s represents the coefficient of sliding friction and Ts is the slip tendency (Collettini and Trippetta, 2007; Morris et al., 1996). Assuming a friction coefficient at the bottom of the Byerlee, 1978 range, $\mu_s = 0.6$, within a seismogenic region, faults with Ts > 0.6 represent structures critically stressed and therefore prone to be easily reactivated (Walsh and Zoback, 2016). The slip tendency depends on the orientation of the fault plane relative to the principal stresses (σ1, σ2 and σ3), the differential stress (σ1 - σ3), the pore fluid pressure and the stress shape ratio φ = (σ2 - σ3/ σ1 - σ3). Because it is difficult to constrain the absolute values of the principal stresses within the seismogenic layer, it is generally used the normalized slip tendency NTs (NTs = Ts/Tsmax) because it depends only on the orientation of the stress tensor and on the stress shape ratio (Morris et al., 1996; Collettini and Trippetta, 2007). NTs = 1 represents the optimal reactivation condition and decreasing values of NTs are indicative of more and more misoriented structures for frictional reactivation: planes with 0.5 < NTs < 1 can be considered well oriented and planes with 0 < NTs < 0.5 are misoriented (Collettini and

Trippetta, 2007).

To evaluate geometric and kinematic compatibility of the reactivated structures within the regional stress field, we calculated the regional stress field using STRESSINVERSE (Vavryčuk, 2014) that is a Matlab software package for an iterative joint inversion for stress and fault orientations from focal mechanisms (Vavryčuk, 2014), based on Michael's method (1984, 1987).

4. Kinematic analysis

4.1. TDMT solutions

The time-space evolution of the AQ and AVN seismic sequences within the GF system in the time interval ranging from April 2009 to February 2017, has been documented in several studies (e.g. Chiaraluce, 2012; Valoroso et al., 2013; Chiaraluce et al., 2017; Michele et al., 2020) and summarized in supplementary material Fig. S3. Here we focus on the geometry and kinematic of the GF and the secondary activated structures.

Fig. 2 shows the focal mechanisms in map colour-coded by sequence: dark green for the 2009 AQ sequence, dark blue for the 2016–2017 AVN sequence and gray for moment tensor solution that do not belong to any sequence. These solutions indicate a prevailing extensional kinematics in agreement with the Appennine active stress field, and the activation of fault areas that do not overlap during both sequences.

In terms of quality, the solutions reviewed in this work have Variance Reduction (VR) values around 60%–80% and have been retrieved by using >4 stations. On average, for events with magnitude Mw < 3.5 the solutions have been computed with 6 stations while for larger events (Mw > 3.5) the solutions have been retrieved by using 10 to 40 stations.

In the study area, due to the adopted ad-hoc 1D wave velocity model for Central Italy and the quite homogeneous azimuthal coverage of the available seismic stations, TDMT solutions are expected to have low CLVD values (Scognamiglio et al., 2009), our solutions confirm this statement having a DC value ranging between 80%–100%.

In the following, to better clarify the geometry and the kinematics of the fault structures, we analyze the seismicity and the retrieved new TDMT solutions in eight cross-sections across the GF in Fig. 3. Fig. 4 highlights the details of main and secondary structures of cross-sections 4, 5 and 8. For a better association of TDMT solutions to the depicted fault structures, we have plotted the TDMT solutions reported in the cross-sections at the corresponding hypocentral depth taken from the Valoroso et al., 2013 (AQ) and Waldhauser et al., 2021 (AVN) catalogs. We did not substitute the depth for those moment tensors showing depth differences larger than 3 km with the catalog-based hypocentral locations, a worsening of the VR value or a change in the kinematics with respect to the obtained TDMT solution.

In cross-section 1 the seismicity is absent along the portion of the GF that hosted the main slip patch of the Amatrice event (see also Fig. S4) and the TDMT solutions belong only to the distributed seismicity located between 7 and 10 km. Here, the extensional kinematics of the solutions do not show a clear low-angle geometry. Moving SE (cross-section 2), the shallower extensional high-angles TDMT well agree with the W-dipping fault plane highlighted by the aftershocks between 1 and 4 km of depth, that well match with the co-seismic slip distribution of Amatrice mainshock from Tinti et al., 2016 (see also Fig. S4). In this cross-

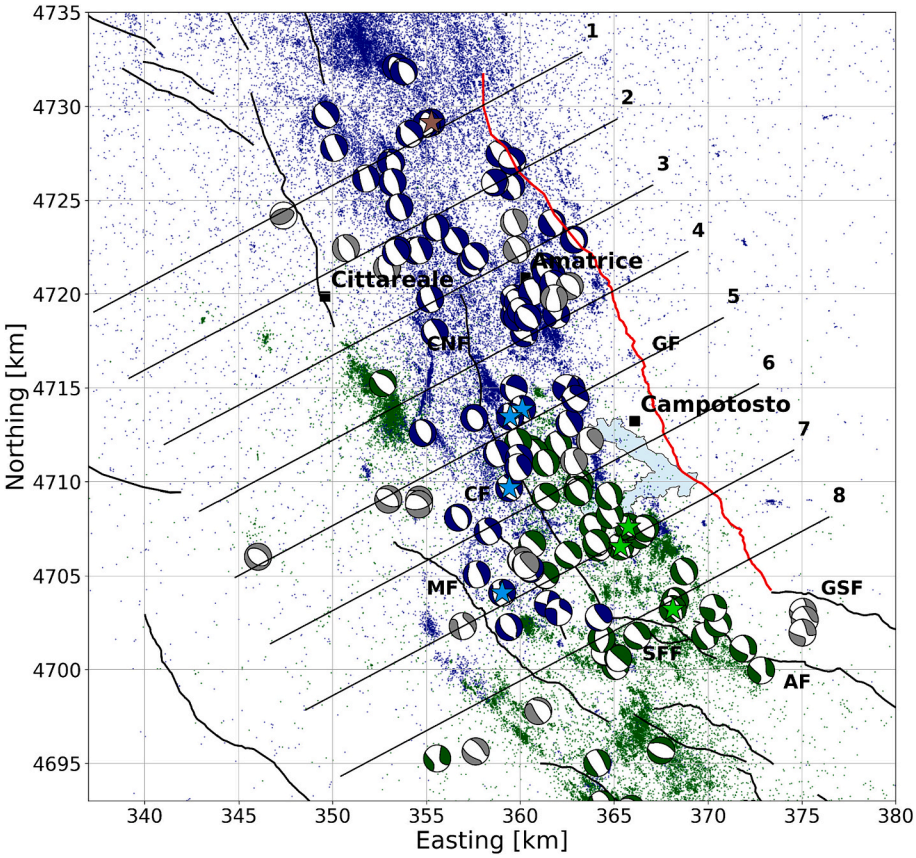

Fig. 2. Map of the study area with calculated TDMT solutions. Dark green solutions belong to the AQ sequence; dark blue solutions belong to the AVN sequence; gray solutions are out-of-sequence. The 8 black solid lines perpendicular to strike of Mw = 5.5 (January 2017) moment tensor solution indicate the location of the cross-sections depicted in Fig. 3. Light blue stars are events with Mw >5.0 of AVN sequence, while light green stars are events with Mw >5.0 of AQ sequence of the Campotosto fault area; brown star is the Amatrice Mw 6.0 mainshock. (For interpretation of the references to colour in this figure legend, the reader is referred to the web version of this article.)

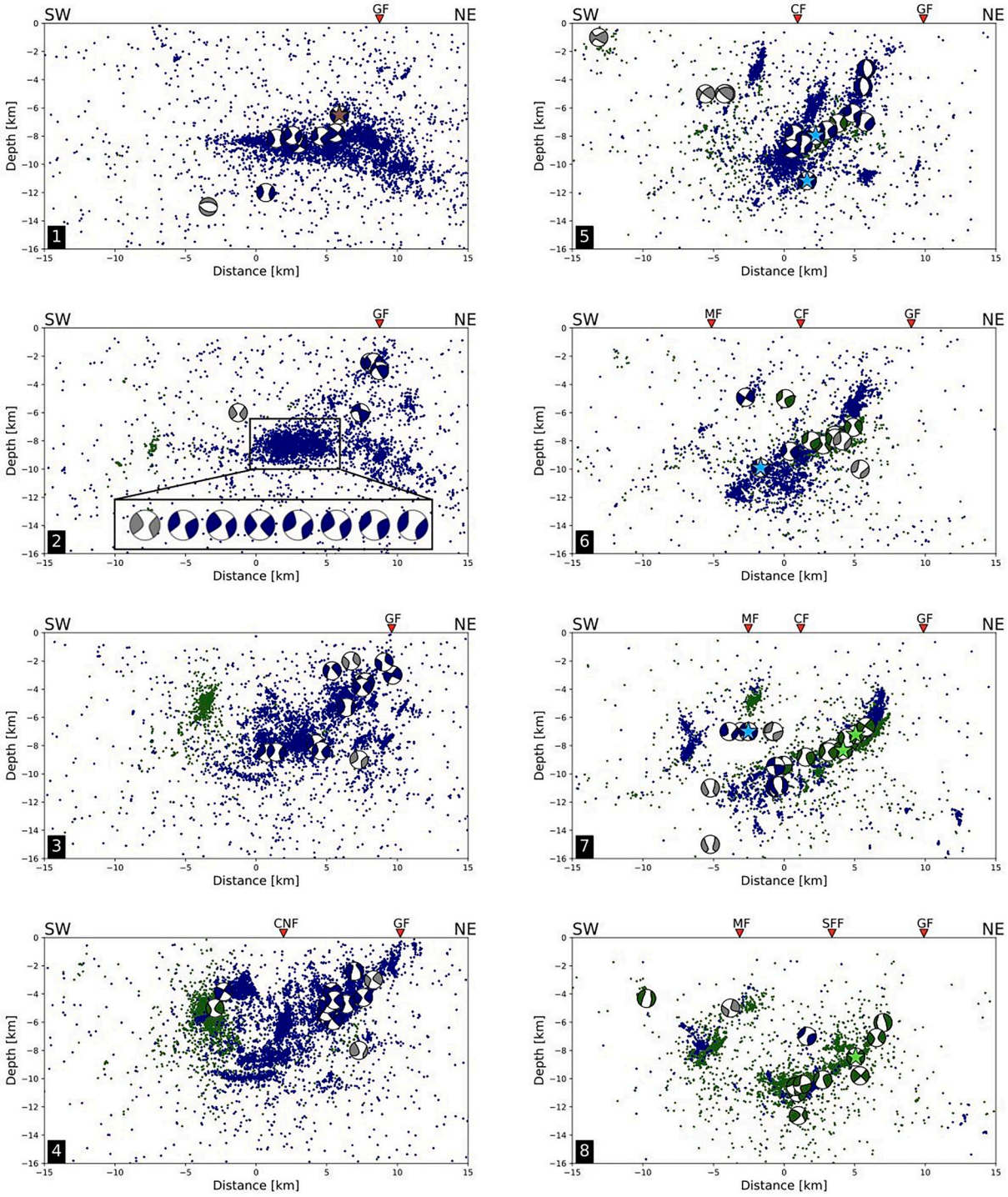

Fig. 3. Set of eight cross-sections. Cross-section traces and fault acronyms are the ones shown in Fig. 2. Moment tensors solutions and seismicity projected in these panels have a distance <2 km from the vertical cross-sections.

section too, the focal mechanisms related to the seismicity volume at depth between 8 and 12 km show an extensional kinematics on normal faults dipping in the range of 25–65°. Cross-Sections 3 and 4 show a seismicity alignment, dipping at 40–50°, that merges at the surface with the mapped GF (Fig. 4). TDMT solutions shallower than 6 km show fault plane parameters in accordance with this seismicity distribution both for the main plane and minor antithetic structures. Cross-Sections 3 and 4 are the southernmost cross-sections where we can observe the sub-horizontal distribution of the seismicity between 8 and 10 km of depth, TDMT related to this seismicity show extensional kinematics (rakes between −80° and − 105°) with strikes in the range 120° - 170° (W or SW dipping planes) and dips 25° - 35°. From cross-section 5, going toward the southern cross-sections, the main fault plane becomes clear. In cross-section 5, the seismicity depicts a GF characterized by a kinked geometry (Chiaraluce, 2012), steeper (65° - 70°) between 2 and 6 km of depth and with smaller inclination (35°- 45°) at depth 6–10 km. This geometry is also confirmed by TDMT solutions (see zoom in Fig. 4). In this cross-section we also observe two strike-slip TDMT solutions dipping 85° and 87° respectively and located at shallow depths. These earthquakes, compatible with the high angle aftershocks distribution,

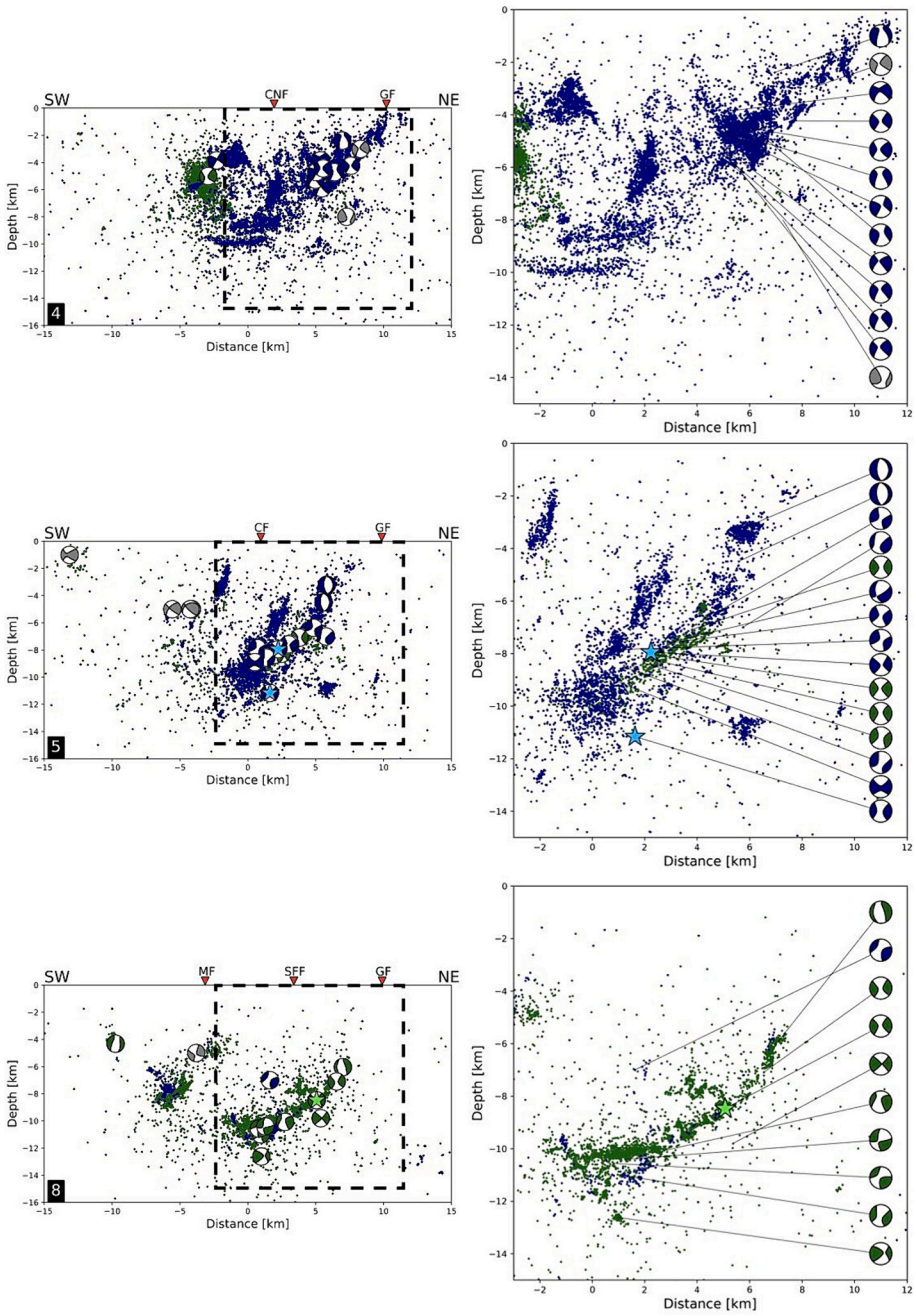

Fig. 4. Zooms of main structures from cross-sections 3, 5 and 8 of Fig. 3.

are probably associated with minor structures that accommodate the overall tectonic deformation. From cross-section 6 to 8, there is a lack of shallow (< 4 km) seismicity. From 4 to 12 km of depth the seismicity distribution highlights a listric geometry that is confirmed by TDMT solutions (Figs. 3 and 4) showing a decrease of the dip-angle with increasing depth (e.g. Chiaraluce, 2012). Seismicity and TDMT distribution shown in Fig. 3, highlight faults that during the AVN sequence were activated in continuity of structures activated during the AQ sequence, with very limited overlapping.

A comprehensive analysis of the ~90 TDMT fault parameters belonging to the GF fault is presented in Fig. 5. Here, within the two nodal planes of the focal mechanisms we have selected the west-dipping ones, as the earthquake fault, because they are coherent with the Gorzano fault plane geometry. Rake values (Fig. 5a) show the predominance of extensional kinematics in agreement with the tectonic regime of the whole area (Chiaraluce et al., 2017). The strike values (Fig. 5b) show a prevalent NW-SE orientation parallel to the axis of the Apennines chain. The dip values (Fig. 5c) highlight a significant variability indicating a clear variation of fault geometry. In Fig. 5d we plot dip angles versus depth only for extensional focal mechanisms to highlight the dip variability potentially related to the main fault geometry of GF. Normal fault solutions have dip angles ranging between (20°-70°). Low-angle dips are distributed between 7 and 11 km of depth, while high angles are between 2 and 7 km (Fig. 5d). This pattern is consistent with the listric and kinked geometry of the Gorzano fault, highlighted also from seismicity and nodal planes distribution (Figs. 3, 4 and S4).

4.2. Slip-tendency results

To obtain the regional stress field, we have inverted the 16 events with M > 4.9 located in the whole area affected by the AQ and AVN sequences in the period 2009–2017 (Table S5).

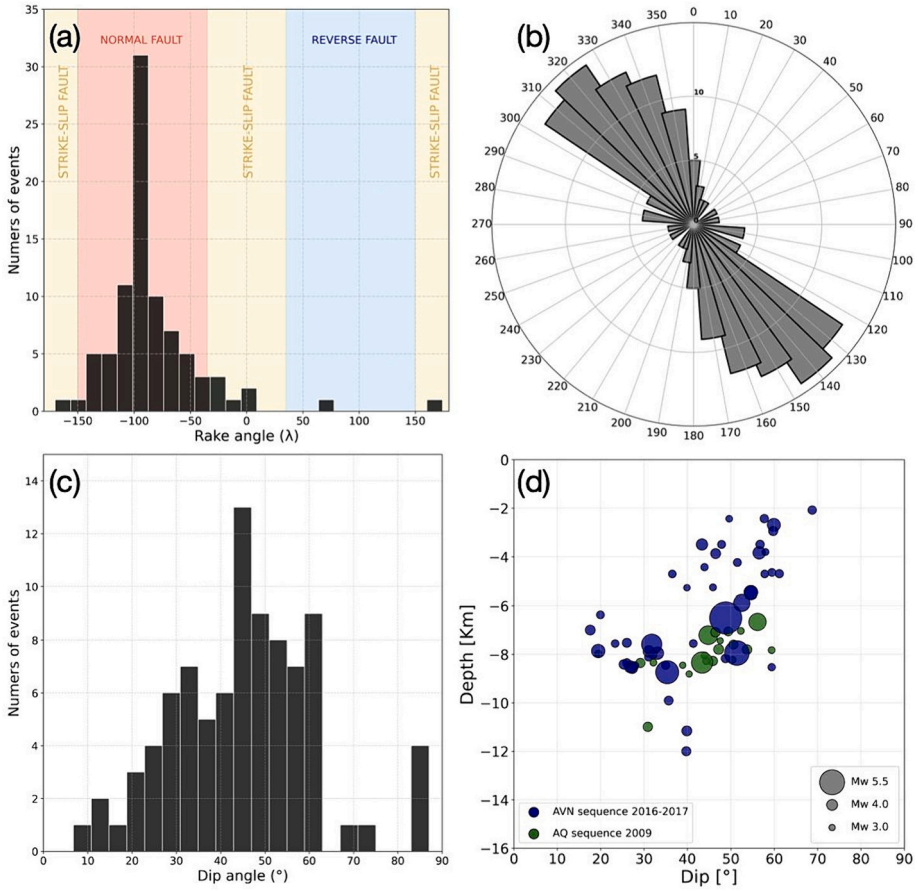

Fig. 5. Results from TDMT solutions belonging to the GF: (a) histogram with rake values; (b) rose diagram with strike values; (c) histogram with dip values; (d) depth versus dip only for normal fault solutions (~120 solutions over 134); the size of dots is related to the magnitude. (For interpretation of the references to colour in this figure legend, the reader is referred to the web version of this article.)

The selection of M > 4.9 implies seismic ruptures larger than some kilometers and therefore not significantly affected by possible local variations in the stress field. The inversion defines values of the stress shape ratio φ and orientation of the principal stress axes $\sigma1$, $\sigma2$, and $\sigma3$ (see Fig. 6a and Table 1).

The $\varphi = 0.58$ obtained in our analysis is consistent with previous works conducted in this area like Boncio et al., 2004b) for the 1992–1994-1996 Campotosto sequences; Chiaraluce et al., 2003) for the 1997 Colfiorito sequence (subvertical $\sigma1$, $\sigma2$ subhorizontal and oriented along the strike of the fault system (NW-SE) and a subhorizontal $\sigma3$ trending NE-SW, resulting in $\varphi = 0.6$.) and (Ferrarini et al., 2015) for the 2009 L'Aquila sequence (Table 1). From φ we can generate the normalized slip-tendency NT_s stereo-plot (Fig. 6b and details in Morris et al., 1996 and Collettini and Trippetta, 2007). To test if our TDMT

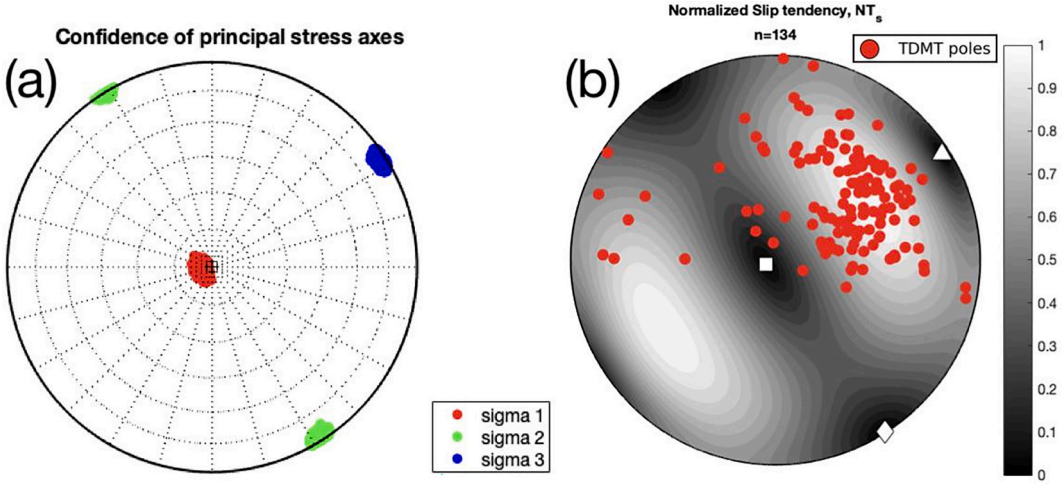

Fig. 6. (a) Principal stress axes plotted into the focal sphere from inversion of events with M > 5.0 between 2009 and 2017. (b) Normalized Slip tendency stereoplot and poles of TDMT solutions (red dots). (For interpretation of the references to colour in this figure legend, the reader is referred to the web version of this article.)

Table 1
Principal stress axes and shape ratio for 16 events with M > 4.9 and comparison with similar analyses.

	σ1	σ2	σ3	φ
M > 5.0 2009–2017 (This study)	245/85	147/0.5	57/04	0.58
Ferrarini et al., 2015	292/85	139/04	48/02	0.56
Boncio et al., 2004b	184/85	344/05	74/02	0.57

solutions are controlled by fault reactivation theory within the regional stress field, obtained from the largest active structures of the area with several km of length, we plot the poles of these solutions on the same stereoplot (red dots in Fig. 6b). From Fig. 6b, it is clear that most of the TDMT solutions are well oriented within the regional stress field (poles representing planes prone to fault reactivation are located in the white areas): 80% of the nodal planes show a $0.7 < NT_s < 1$, 16% a $0.4 < NT_s < 0.7$ and only 4% have NTs < 0.4.

5. Discussion

The Gorzano fault, GF, is a large and active normal fault within the seismically active area of the Apennines that was only partially reactivated during the last two seismic sequences AQ 2009 and AVN 2016–2017. In the following we firstly reconstruct a mechanical model to discuss the GF slip behavior, and then we expand the discussion on the possible style of reactivation of the GF.

The mechanical model (Fig. 7) is reconstructed integrating surface and subsurface geology (Porreca et al., 2018; Barchi et al., 2021) and laboratory friction experiments (Scuderi et al., 2013; Carpenter et al., 2014; Scuderi et al., 2020; Pozzi et al., 2022). Surface geology and seismic reflection profiles show that the first ~2 km of the fault are contained within the Laga (Late Miocene) formation. The predominance of clay minerals within this formation promotes a velocity strengthening (VS) frictional behavior (Ikari et al., 2009; Scuderi and Collettini, 2018). This means that earthquake nucleation on this shallow fault portion is extremely unlikely (Marone, 1998; Scholz, 2019) and rupture propagation at first approximation tends to be inhibited (Kaneko et al., 2010). In the depth-range of 2–9 km, Mesozoic-Paleogene carbonates and Triassic Evaporites are present (Barchi et al., 2021). Laboratory friction experiments on these fault rocks indicate that strain localization along the fault favors a velocity weakening (VW) frictional behavior (Scuderi et al., 2013; Carpenter et al., 2014; Scuderi et al., 2020; Pozzi et al., 2022). A velocity weakening behavior means that earthquake nucleation on these lithologies is possible. At depth > 9 km seismic reflection

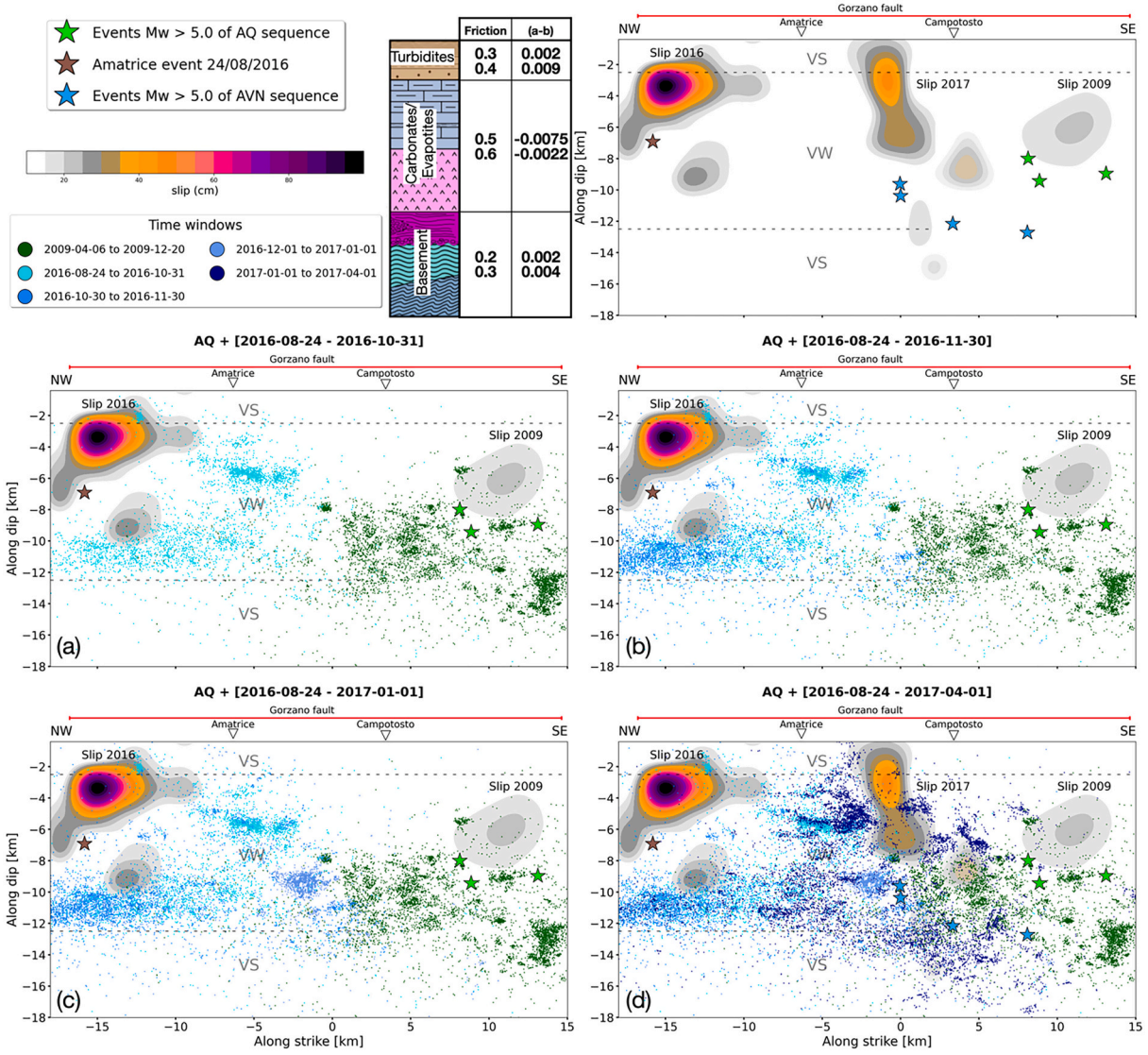

Fig. 7. Seismic and slip distribution within ±1.5 km on Gorzano fault plane, with 50° of dip and 152° of strike, through four-time windows (details are in the legend). For the AVN catalog only events with magnitude Mw > 0.5 are considered. Stratigraphic column from Volpe et al., 2022.

profiles (Barchi et al., 2021) indicate the presence of the acoustic basement. For the SE portion of the fault, seismic profiles are not available and therefore the characterization of fault rocks at these depths is not well constrained. The acoustic basement is rich in phyllosilicates and laboratory studies on fault rocks analogues of the Apenninic basement, define a velocity strengthening behavior pointing to stable sliding and fault creep (Volpe et al., 2022, 2023). To summarize and present all the collected information and dataset in a comprehensive picture of the GF we integrate (Fig. 7):

1) the events of the AQ (green dots) and AVN (shades of blue) sequences located within +/− 1.5 km from the Gorzano fault plane (orthogonal distance), with 50° of dip and 152° of strike, as constrained from the focal mechanism of the M 5.5 mainshock of January 2017.

2) the coseismic slip for the major earthquakes occurring along the fault, that are: the cumulative coseismic and postseismic slip of M > 5.0 events nucleating during the 2009 AQ sequence (Cheloni et al., 2014); the southern slip patch of the Amatrice Mw 6.0, 24 August 2016 mainshock (Tinti et al., 2016); and the cumulative coseismic slip of two M > 5.4 events occurred on 18 January 2017 (Cheloni et al., 2019).

3) the inferred frictional properties and slip behavior for the GF at different depths (indicated in Fig. 7 with VS and VW). Details in the average frictional properties for the rocks composing the seismogenic layer are reported in Fig. 7 next the stratigraphic column.

The different panels in Fig. 7 show the seismicity and slip distribution on the fault plane through four-time windows indicated in the legend. The SE portion of the GF started to be reactivated during the AQ 2009 sequence (Fig. 7a). The homogeneously distributed seismicity in the depth range 7.5–12.5 km represents the reactivation of this portion of the GF well-imaged in cross-sections 6–8 of Fig. 3. The deeper clustering of the seismicity at 12–15 km along dip (that corresponds to 9–12 km of depth) in the SE termination of the fault highlights the gently dipping lower portion of the GF (cf. also cross-section 8 of Figs. 3 and 4). The cumulative slip of the three M > 5.0 events of the 2009 AQ sequence is located up-dip from the mainshocks and shows a limited aftershock activity in the dislocated area and adjacent areas at shallow depths. On the contrary some clusters of seismicity occur around the slipped area at larger depths. During the 2016 AVN the NW termination of the GF, started to be reactivated with the Amatrice mainshock. The earthquake released a first main slip patch (equivalent Mw 5.8), with up to 1 m of coseismic slip, up-dip from the hypocenter (Fig. 7a) and then propagated northwards onto the southern portion of the Vettore fault releasing a second extended slip patch (not shown here) equivalent to Mw 5.95 (Tinti et al., 2016). In the slip patch hosted within the GF, we observe again the absence of aftershock activity around the slipped area. Most of the early aftershocks of Amatrice occurs at 8–12 km along dip (equivalent to a depth range of ~6–10 km, see also Fig. 3 cross-sections 1–2) where the GF likely merge at depth into a distributed horizontal seismicity interpreted as an extensional detachment (Waldhauser et al., 2021) or distributed deformation within the Triassic Evaporites (Collettini et al., 2022). At shallower crustal levels (Fig. 7a at coordinates −4-7 km along dip and centered at −5 km along strike), where the Amatrice slipped area ends, an intense and aligned aftershock activity highlights a portion of the GF and a small antithetic fault (cf. cross-section 4 in Fig. 3). In the month following the Norcia Mw 6.5 mainshock (Fig. 7b), we observe that the seismicity persists in the fault portions activated by the Amatrice aftershocks and a limited aftershock activity occurs within the Amatrice slip patch. During December 2016, aftershock activity still occurs in the fault portions reactivated by Amatrice and Norcia, but we also observe that seismicity is now concentrating along a portion of the GF (Fig. 7c center at coordinates −9 km along dip and − 4–0 km along strike) not previously illuminated by seismic activity. This seismicity connects the GF fault areas activated during the AQ and the first 4 months of the AVN sequence. At the SE termination of this activated fault portion, on 18 January 2017 two of the four M > 5.0 events that affected this area during the AVN sequence, nucleate (Fig. 7d). Here again we observe that the cumulative coseismic slip of the two mainshocks is concentrated up-dip of the hypocenters and that aftershocks occurrence is mostly concentrated around the perimeter of the slipped area. Co-seismic slip shows an extremely consistent picture of the dislocation occurred along the main GF structure, with slip distributed from the mainshocks, up-dip until the fault mapped at the surface (see also cross-section 5 in Fig. 3). These data strongly support the seismic activity of the mapped GF (e.g., Galadini and Galli, 2003; Boncio et al., 2004a; Lavecchia et al., 2012; Falcucci et al., 2018; Waldhauser et al., 2021) and contradicts the interpretation that the shallow portion of the GF is cut and passively transported by a regional thrust belonging to the previously developed Pliocene compressional phase (Buttinelli et al., 2021).

At first approximation the integration of seismological data with inferred frictional properties of the GF depicts a coherent picture of a fault that is partially reactivated during the AQ 2009 and AVN 2016 seismic sequences (Fig. 7d). Starting from the AQ sequence, this partial reactivation occurs in a way that allows reactivation only along fault portions that did not experience previous coseismic fault slip or aftershock occurrence. Most of the seismicity occurs at depth of 2–9 km and nucleates within the Carbonates and Triassic Evaporites where the frictional velocity weakening behavior of the fault rocks well explains earthquake nucleation. The velocity strengthening behavior of the: a) clay rich lithologies of the Laga formation at shallow, 1–2 km, crustal levels and 2) the phyllosilicates of the basement at depth > 9–10 km in the NW portion of the fault, further support aftershock confinement in the depth-range of 2–9 km. Most of the co-seismic slip is contained within the 2–9 km depth range, with some propagation of the co-seismic slip at shallow crustal levels where velocity strengthening fault rocks are likely present. An explanation for this can be related to possible dynamic weakening processes occurring within fault rocks characterized by a velocity strengthening behavior (e.g., Faulkner et al., 2011; Noda and Lapusta, 2013), or to the presence of more competent quartz-rich domains within the Laga formation (Centamore and Terra, 1992) or simply to a gradual rupture arrest on the velocity strengthening region (Tinti et al., 2005).

Is the partial reactivation of separated and different fault portions the only style of rupture behavior for the GF? In this second part of the discussion, we are going to merge observations from different case studies with our dataset to address the above question. Examples of seismic ruptures that jumped from one segment to another, in geometric and kinematic boundary conditions more unfavorable in comparison to the GF, are becoming more and more documented in the literature. Two earthquakes with Mw = 8.4 and Mw = 7.9, occurred in the Sumatra megathrust in 2007 within a 12-h interval, ruptured only a fraction of the 1833 event area (Mw = 9.0) indicating that the same fault can rupture in different ways, depending on whether asperities dislocate as isolated or cooperate to produce a larger rupture (Konca et al., 2008). On February 6, 2023, a Mw = 7.8 earthquake struck south-central Turkey, and was followed by a Mw 6.7 aftershock (~ 11 min later) and a Mw 7.5 (~ 9 h later) which struck 95 km to the north on a distinct fault, probably triggered by stress transfer (Dal Zilio and Ampuero, 2023). For the Mw = 7.8, 2016 Kaikoura earthquake in New Zealand, geodetic and field observations suggest earthquake rupture along at least 12 major faults belonging to two distinct tectonic domains (strike and reverse slip respectively), with step-over of 15–20 km (Hamling et al., 2017). In central Italy the 1997–1998 Colfiorito seismic sequence is characterized by 3 major ruptures (5.6 < M < 6.0) that are limited by inherited compressional structures (Collettini et al., 2005) whereas for the 2016–2017 seismic sequence the same inherited compressional structures acted as sites for stress concentrations, where the major ruptures easily passed through (Pizzi et al., 2017; Scognamiglio et al., 2018). For the GF, our geometrical and mechanical reconstruction defines a large single structure with some geometrical (change in fault dip with depth) and frictional (see the model of Fig. 7) heterogeneities. The kinematics analysis depicts the GF as an optimally oriented fault within the regional stress field and Slip Tendency indicates that small GF

portions, or associated structures, are well oriented for frictional reactivation. All together these data support a possible complete reactivation of the fault, capable of a M 6.5–6.6 earthquake, as documented in paleoseismological data (Galadini and Galli, 2003). This is also consistent with the above reported observations indicating that seismic ruptures in the same area may differ significantly and rupture jumps can be very efficient and sometimes difficult to predict. We suggest that the partial reactivation of the fault observed in the time 2009–2017 can be related to the documented geometrical and frictional heterogeneities together with a stress level approaching that of failure in different time periods (Tinti et al., 2021). However, due to the geometric and kinematic similarities of the different fault portions, under more favorable stress conditions the entire fault reactivation of the fault cannot be excluded.

6. Conclusion

Thanks to the integration of a new TDMT catalog with seismicity catalogs and slip distribution models from previous works (Waldhauser et al., 2021; Valoroso et al., 2013; Tinti et al., 2016; Cheloni et al., 2019; Cheloni et al., 2014), it was possible to characterize the geometry and kinematic of the Gorzano fault, that hosted several M > 5.0 earthquakes during the last two major sequences of Central Italy. The studied 134 TDMT solutions suggest that these events occurred on a SW-dipping normal fault, characterized by a fault structure with a planar geometry and dipping at about 50° in the north portion. Moving southward, the fault has a listric geometry, decreasing its dip with depth and reaching a dip of about 20° at ~8 km. Synthetic and antithetic structures are widespread and in some portions the base of the GF merges into a zone of distributed seismicity at 8–10 km.

To discuss the possible slip behavior of the GF, we have developed a mechanical model integrating seismological data with inferred frictional properties of the seismogenic layer. The GF is an optimally oriented fault within the regional stress field and Slip Tendency analysis shows that small GF portions are well oriented for frictional reactivation. From 2009 to 2017, the reactivation, via aftershock or mainshock slip, of complementary fault portions of the entire GF indicates that the fault behaves as a single fault structure. Between 2 and 9 km of depth the rate weakening behavior of the carbonates of the Apennines well explain mainshock nucleation and abundant aftershock occurrence along adjacent fault segments. Geometrical, different fault dips, and frictional heterogeneities can be at the base of the GF slip behavior observed in the last 30 years, that is reactivation of different fault portions with 5.0 < M < 6.0. However, the entire structure is well oriented within the regional stress field and for extremely favorable initial stress conditions, a seismic rupture reactivating the fault for its entire length cannot be excluded.

CRediT authorship contribution statement

M.E. Locchi: Writing – original draft, Formal analysis, Data curation, Conceptualization. **L. Scognamiglio:** Conceptualization, Formal analysis, Supervision, Writing – review & editing. **E. Tinti:** Writing – review & editing, Supervision, Formal analysis, Conceptualization. **C. Collettini:** Formal analysis, Conceptualization, Supervision, Writing – review & editing.

Declaration of competing interest

The authors declare that they have no known competing financial interests or personal relationships that could have appeared to influence the work reported in this paper.

Data availability

The seismicity catalog for AVN used in this work is published in Waldhauser et al., 2021, and access can be obtained at the Zenodo dataset repository (https://zenodo.org/records/5091137). The seismicity catalog for AQ used in this work is published in Valoroso et al., 2013 and available at the Zenodo dataset repository (https://zenodo.org/records/4036248). The TDMT solutions are available on Table S1 of supplementary materials and at the Zenodo repository https://doi.org/10.5281/zenodo.10801577. The Normalized Slip tendency is computed with STRESSINVERSE Matlab software is available in the following link https://www.ig.cas.cz/stress-inverse/.

Acknowledgments

We thank the editor C. A. Currie and the anonymous reviews for their helpful and detailed reviews. Authors wish to acknowledge the financial support provided by the PNRR funding scheme (Piano Nazionale di Ripresa e Resilienza, in Italian) as part of the National Research Centre CN1 on “High-Performance Computing, Big Data and Quantum Computing” - Spoke 5 - Environment and Natural Disaster: Framework and methodologies for impact evaluation and risk mitigation, whose support is greatly appreciated.

Appendix A. Supplementary data

Supplementary data to this article can be found online at https://doi.org/10.1016/j.tecto.2024.230284.

References

Anderlini, L., Serpelloni, E., Belardinelli, M.E., 2016. Creep and locking of a low-angle normal fault: Insights from the Altotiberina fault in the northern Apennines (Italy). Geophys. Res. Lett. 43 (9), 4321–4329. https://doi.org/10.1002/2016GL068604.

Barbot, S., 2019. Slow-slip, slow earthquakes, period-two cycles, full and partial ruptures, and deterministic chaos in a single asperity fault. Tectonophysics 768, 228171. https://doi.org/10.1016/j.tecto.2019.228171.

Barbot, S., 2021. A spectral boundary-integral method for quasi-dynamic ruptures of multiple parallel faults. Bull. Seismol. Soc. Am. 111 (3), 1614–1630. https://doi.org/10.1785/0120210004.

Barchi, M.R., Carboni, F., Michele, M., Ercoli, M., Giorgetti, C., Porreca, M., Chiaraluce, L., 2021. The influence of subsurface geology on the distribution of earthquakes during the 2016-–2017 Central Italy seismic sequence. Tectonophysics 807, 228797. https://doi.org/10.1016/j.tecto.2021.228797.

Biasi, G.P., Wesnousky, S.G., 2016. Steps and gaps in ground ruptures: Empirical bounds on rupture propagation. Bull. Seismol. Soc. Am. 106 (3), 1110–1124. https://doi.org/10.1785/0120150175.

Bigi, S., Casero, P., Ciotoli, G., 2011. Seismic interpretation of the Laga basin; constraints on the structural setting and kinematics of the Central Apennines. J. Geol. Soc. Lond. 168 (1), 179–190. https://doi.org/10.1144/0016-76492010-084.

Boncio, P., Lavecchia, G., Pace, B., 2004a. Defining a model of 3D seismogenic sources for Seismic Hazard Assessment applications: the case of central Apennines (Italy). J. Seismol. 8, 407–426. https://doi.org/10.1023/B:JOSE.0000038449.78801.05.

Boncio, P., Lavecchia, G., Milana, G., Rozzi, B., 2004b. Seismogenesis in Central Apennines, Italy: an integrated analysis of minor earthquake sequences and structural data in the Amatrice-Campotosto area. Ann. Geophys. 47 (6), 1723–1743. http://hdl.handle.net/2122/865.

Buttinelli, M., Petracchini, L., Maesano, F.E., D'Ambrogi, C., Scrocca, D., Marino, M., DI Bucci, D., 2021. The impact of structural complexity, fault segmentation, and reactivation on seismotectonics: Constraints from the upper crust of the 2016–2017 Central Italy seismic sequence area. Tectonophysics 810, 228861. https://doi.org/10.1016/j.tecto.2021.228861.

Byerlee, J., 1978. Friction of rocks. Rock Frict. Earthqu. Predict. 615–626.

Carpenter, B.M., Scuderi, M.M., Collettini, C., Marone, C., 2014. Frictional heterogeneities on carbonate-bearing normal faults: Insights from the Monte Maggio Fault, Italy. J. Geophys. Res. Solid Earth 119 (12), 9062–9076. https://doi.org/10.1002/2014JB011337.

Centamore, E., Terra, U.D., 1992. Carta geologica dei bacini della Laga e del Cellino e dei rilievi carbonatici circostanti (Marche Meridionali). Lazio nord-Orientale, Abruzzo settentrionale.

Cheloni, D., Giuliani, R., D'Anastasio, E., Atzori, S., Walters, R.J., Bonci, L., Stefanelli, G., 2014. Coseismic and post-seismic slip of the 2009 L'Aquila (Central Italy) MW 6.3 earthquake and implications for seismic potential along the Campotosto fault from joint inversion of high-precision levelling, InSAR and GPS data. Tectonophysics 622, 168–185. https://doi.org/10.1016/j.tecto.2014.03.009.

Cheloni, D., D'Agostino, N., Scognamiglio, L., Tinti, E., Bignami, C., Avallone, A., Mattone, M., 2019. Heterogeneous behavior of the Campotosto normal fault (Central Italy) imaged by InSAR GPS and strong-motion data: Insights from the 18 January 2017 events. Remote Sens. 11 (12), 1482. https://doi.org/10.3390/rs11121482.

Chiarabba, C., Amato, A., Anselmi, M., Baccheschi, P., Bianchi, I., Cattaneo, M., Valoroso, L., 2009. The 2009 L'Aquila (Central Italy) MW6. 3 earthquake: Main

shock and aftershocks. Geophys. Res. Lett. 36 (18) https://doi.org/10.1029/2009GL039627.
Chiaraluce, L., 2012. Unravelling the complexity of Apenninic extensional fault systems: a review of the 2009 L'Aquila earthquake (Central Apennines, Italy). J. Struct. Geol. 42, 2–18. https://doi.org/10.1016/j.jsg.2012.06.007.
Chiaraluce, L., Ellsworth, W.L., Chiarabba, C., Cocco, M., 2003. Imaging the complexity of an active normal fault system: the 1997 Colfiorito (Central Italy) case study. J. Geophys. Res. Solid Earth 108 (B6). https://doi.org/10.1029/2002JB002166.
Chiaraluce, L., Di Stefano, R., Tinti, E., Scognamiglio, L., Michele, M., Casarotti, E., Marzorati, S., 2017. The 2016 Central Italy seismic sequence: a first look at the mainshocks, aftershocks, and source models. Seismol. Res. Lett. 88 (3), 757–771. https://doi.org/10.1785/0220160221.
Collettini, C., Trippetta, F., 2007. A slip tendency analysis to test mechanical and structural control on aftershock rupture planes. Earth Planet. Sci. Lett. 255 (3–4), 402–413. https://doi.org/10.1016/j.epsl.2007.01.001.
Collettini, C., Chiaraluce, L., Pucci, S., Barchi, M.R., Cocco, M., 2005. Looking at fault reactivation matching structural geology and seismological data. J. Struct. Geol. 27 (5), 937–942. https://doi.org/10.1016/j.jsg.2004.10.016.
Collettini, C., Barchi, M.R., De Paola, N., Trippetta, F., Tinti, E., 2022. Rock and fault rheology explain differences between on fault and distributed seismicity. Nat. Commun. 13 (1), 5627. https://doi.org/10.1038/s41467-022-33373-y.
Dal Zilio, L., Ampuero, J.P., 2023. Earthquake doublet in Turkey and Syria. Communicat. Earth & Environ. 4 (1), 71. https://doi.org/10.1038/s43247-023-00747-z.
Dreger, D.S., Helmberger, D.V., 1993. Determination of source parameters at regional distances with three-component sparse network data. J. Geophys. Res. Solid Earth 98 (B5), 8107–8125. https://doi.org/10.1029/93JB00023.
Falcucci, E., Gori, S., Bignami, C., Pietrantonio, G., Melini, D., Moro, M., Galadini, F., 2018. The Campotosto seismic gap in between the 2009 and 2016–2017 seismic sequences of Central Italy and the role of inherited lithospheric faults in regional seismotectonic settings. Tectonics 37 (8), 2425–2445. https://doi.org/10.1029/2017TC004844.
Faulkner, D.R., Mitchell, T.M., Jensen, E., Cembrano, J., 2011. Scaling of fault damage zones with displacement and the implications for fault growth processes. J. Geophys. Res. Solid Earth 116 (B5). https://doi.org/10.1029/2010JB007788.
Ferrarini, F., Lavecchia, G., de Nardis, R., Brozzetti, F., 2015. Fault geometry and active stress from earthquakes and field geology data analysis: the Colfiorito 1997 and L'Aquila 2009 cases (Central Italy). Pure Appl. Geophys. 172, 1079–1103. https://doi.org/10.1007/s00024-014-0931-7.
Galadini, F., Galli, P., 2003. Paleoseismology of silent faults in the Central Apennines (Italy): the Mt. Vettore and Laga Mts. Faults. Ann. Geophys. 46 (5), 815–836. http://hdl.handle.net/2122/991.
Gallovič, F., Valentová, L., Ampuero, J.P., Gabriel, A.A., 2019. Bayesian dynamic finite-fault inversion: 2. Application to the 2016 Mw 6.2 Amatrice, Italy, earthquake. J. Geophys. Res. Solid Earth 124 (7), 6970–6988. https://doi.org/10.1029/2019JB017510.
Hamling, I.J., Hreinsdóttir, S., Clark, K., Elliott, J., Liang, C., Fielding, E., Stirling, M., 2017. Complex multifault rupture during the 2016 M w 7.8 Kaikōura earthquake, New Zealand. Science 356 (6334), eaam7194. https://doi.org/10.1126/science.aam7194.
Ikari, M.J., Saffer, D.M., Marone, C., 2009. Frictional and hydrologic properties of clay-rich fault gouge. J. Geophys. Res. Solid Earth 114 (B5). https://doi.org/10.1029/2008JB006089.
Kaneko, Y., Avouac, J.P., Lapusta, N., 2010. Towards inferring earthquake patterns from geodetic observations of interseismic coupling. Nat. Geosci. 3 (5), 363–369. https://doi.org/10.1038/ngeo843.
Konca, A., Avouac, J.P., Sladen, A., Meltzner, A.J., Sieh, K., Fang, P., Helmberger, D.V., 2008. Partial rupture of a locked patch of the Sumatra megathrust during the 2007 earthquake sequence. Nature 456 (7222), 631–635. https://doi.org/10.1038/nature07572.
Lavecchia, G., Brozzetti, F., Barchi, M.R., Menichetti, M., Keller, J.V., 1994. Seismotectonic zoning in east-Central Italy deduced from an analysis of the Neogene to present deformations and related stress fields. Geol. Soc. Am. Bull. 106 (9), 1107–1120. https://doi.org/10.1130/0016-7606(1994)106<1107:SZIECI>2.3.CO;2.
Lavecchia, G., Ferrarini, F., Brozzetti, F., De Nardis, R., Boncio, P., Chiaraluce, L., 2012. From surface geology to aftershock analysis: Constraints on the geometry of the L'Aquila 2009 seismogenic fault system. Ital. J. Geosci. 131 (1) https://doi.org/10.3301/IJG.2012.24, 330–247.
Marone, C., 1998. Laboratory-derived friction laws and their application to seismic faulting. Annu. Rev. Earth Planet. Sci. 26 (1), 643–696. https://doi.org/10.1146/annurev.earth.26.1.643.
Michele, M., Chiaraluce, L., Di Stefano, R., Waldhauser, F., 2020. Fine-scale structure of the 2016–2017 Central Italy seismic sequence from data recorded at the Italian National Network. J. Geophys. Res. Solid Earth 125 (4). https://doi.org/10.1029/2019JB018440 e2019JB018440.
Morris, A., Ferrill, D.A., Henderson, D.B., 1996. Slip-tendency analysis and fault reactivation. Geology 24 (3), 275–278. https://doi.org/10.1130/0091-7613(1996)024<0275:STAAFR>2.3.CO;2.
Noda, H., Lapusta, N., 2013. Stable creeping fault segments can become destructive as a result of dynamic weakening. Nature 493 (7433), 518–521. https://doi.org/10.1038/nature11703.
Pasyanos, M.E., Dreger, D.S., Romanowicz, B., 1996. Toward real-time estimation of regional moment tensors. Bull. Seismol. Soc. Am. 86 (5), 1255–1269. https://doi.org/10.1785/BSSA0860051255.
Pizzi, A., Galadini, F., Pizzi, A., Galadini, F., 2009. Pre-existing cross-structures and active fault segmentation in the northern-central Apennines (Italy). Tectonophysics 476 (1–2), 304–319. https://doi.org/10.1016/j.tecto.2009.03.018.
Pizzi, A., Di Domenica, A., Gallovič, F., Luzi, L., Puglia, R., 2017. Fault segmentation as constraint to the occurrence of the main shocks of the 2016 Central Italy seismic sequence. Tectonics 36 (11), 2370–2387. https://doi.org/10.1002/2017TC004652.
Porreca, M., Minelli, G., Ercoli, M., Brobia, A., Mancinelli, P., Cruciani, F., Barchi, M.R., 2018. Seismic reflection profiles and subsurface geology of the area interested by the 2016–2017 earthquake sequence (Central Italy). Tectonics 37 (4), 1116–1137. https://doi.org/10.1002/2017TC004915.
Pozzi, G., Scuderi, M.M., Tinti, E., Nazzari, M., Collettini, C., 2022. The role of fault rock fabric in the dynamics of laboratory faults. J. Geophys. Res. Solid Earth 127 (6). https://doi.org/10.1029/2021JB023779 e2021JB023779.
Scholz, C.H., 2010. Large earthquake triggering, clustering, and the synchronization of faults. Bull. Seismol. Soc. Am. 100 (3), 901–909. https://doi.org/10.1785/0120090309.
Scholz, C.H., 2019. The Mechanics of Earthquakes and Faulting. Cambridge University Press.
Scholz, C.H., Gupta, A., 2000. Fault interactions and seismic hazard. J. Geodyn. 29 (3–5), 459–467. https://doi.org/10.1016/S0264-3707(99)00040-X.
Scognamiglio, L., Tinti, E., Michelini, A., 2009. Real-time determination of seismic moment tensor for the Italian region. Bull. Seismol. Soc. Am. 99 (4), 2223–2242. https://doi.org/10.1785/0120080104.
Scognamiglio, L., Tinti, E., Casarotti, E., Pucci, S., Villani, F., Cocco, M., Dreger, D.S., 2018. Complex fault geometry and rupture dynamics of the MW 6.5, 30 October 2016a, Central Italy earthquake. J. Geophys. Res. Solid Earth 123 (4), 2943–2964. https://doi.org/10.1002/2018JB015603.
Scuderi, M.M., Collettini, C., 2018. Fluid injection and the mechanics of frictional stability of shale-bearing faults. J. Geophys. Res. Solid Earth 123 (10), 8364–8384. https://doi.org/10.1029/2018JB016084.
Scuderi, M.M., Niemeijer, A.R., Collettini, C., Marone, C., 2013. Frictional properties and slip stability of active faults within carbonate–evaporite sequences: the role of dolomite and anhydrite. Earth Planet. Sci. Lett. 369, 220–232. https://doi.org/10.1016/j.epsl.2013.03.024.
Scuderi, M.M., Tinti, E., Cocco, M., Collettini, C., 2020. The role of shear fabric in controlling breakdown processes during laboratory slow-slip events. J. Geophys. Res. Solid Earth 125 (11). https://doi.org/10.1029/2020JB020405 e2020JB020405.
Serpelloni, E., Anzidei, M., Baldi, P., Casula, G., Galvani, A., 2005. Crustal velocity and strain-rate fields in Italy and surrounding regions: new results from the analysis of permanent and non-permanent GPS networks. Geophys. J. Int. 161 (3), 861–880. https://doi.org/10.1111/j.1365-246X.2005.02618.x.
Sibson, S.H., 1985. Stopping of earthquake ruptures at dilational fault jogs. Nature 316 (6025), 248–251. https://doi.org/10.1038/316248a0.
Spallarossa, D., Cattaneo, M., Scafidi, D., Michele, M., Chiaraluce, L., Segou, M., Main, I. G., 2021. An automatically generated high-resolution earthquake catalogue for the 2016–2017 Central Italy seismic sequence, including P and S phase arrival times. Geophys. J. Int. 225 (1), 555–571. https://doi.org/10.1093/gji/ggaa604.
Thomas, M.Y., Lapusta, N., Noda, H., Avouac, J.P., 2014. Quasi-dynamic versus fully dynamic simulations of earthquakes and aseismic slip with and without enhanced coseismic weakening. J. Geophys. Res. Solid Earth 119 (3), 1986–2004. https://doi.org/10.1002/2013JB010615.
Tinti, E., Fukuyama, E., Piatanesi, A., Cocco, M., 2005. A kinematic source-time function compatible with earthquake dynamics. Bull. Seismol. Soc. Am. 95 (4), 1211–1223. https://doi.org/10.1785/0120040177.
Tinti, E., Scognamiglio, L., Michelini, A., Cocco, M., 2016. Slip heterogeneity and directivity of the ML 6.0, 2016, Amatrice earthquake estimated with rapid finite-fault inversion. Geophys. Res. Lett. 43 (20), 10–745. https://doi.org/10.1002/2016GL071263.
Tinti, E., Casarotti, E., Ulrich, T., Taufiqurrahman, T., Li, D., Gabriel, A.A., 2021. Constraining families of dynamic models using geological, geodetic and strong ground motion data: The Mw 6.5, October 30th, 2016, Norcia earthquake, Italy. Earth Planet. Sci. Lett. 576, 117237. https://doi.org/10.1016/j.epsl.2021.117237.
Valoroso, L., Chiaraluce, L., Piccinini, D., Di Stefano, R., Schaff, D., Waldhauser, F., 2013. Radiography of a normal fault system by 64,000 high-precision earthquake locations: the 2009 L'Aquila (Central Italy) case study. J. Geophys. Res. Solid Earth 118 (3), 1156–1176. https://doi.org/10.1002/jgrb.50130.
Vavryčuk, V., 2014. Iterative joint inversion for stress and fault orientations from focal mechanisms. Geophys. J. Int. 199 (1), 69–77. https://doi.org/10.1093/gji/ggu224.
Villani, F., Pucci, S., Civico, R., De Martini, P.M., Cinti, F.R., Piantosti, D., 2018. Surface faulting of the 30 October 2016 Mw 6.5 central Italy earthquake: Detailed analysis of a complex coseismic rupture. Tectonics 37 (10), 3378–3410.
Volpe, G., Pozzi, G., Collettini, C., 2022. YBPR or SCC′? Suggestion for the nomenclature of experimental brittle fault fabric in phyllosilicate-granular mixtures. J. Struct. Geol. 165, 104743 https://doi.org/10.1016/j.jsg.2022.104743.
Volpe, G., Pozzi, G., Collettini, C., Spagnuolo, E., Achtziger-Zupančič, P., Zappone, A., Cocco, M., 2023. Laboratory simulation of fault reactivation by fluid injection and implications for induced seismicity at the BedrettoLab, Swiss Alps. Tectonophysics 862, 229987. https://doi.org/10.1016/j.tecto.2023.229987.
Waldhauser, F., Michele, M., Chiaraluce, L., Di Stefano, R., Schaff, D.P., 2021. Fault planes, fault zone structure and detachment fragmentation resolved with high-precision aftershock locations of the 2016–2017 Central Italy sequence. Geophys. Res. Lett. 48 (16) https://doi.org/10.1029/2021GL092918 e2021GL092918.
Walsh, F.R., Zoback, M.D., 2016. Probabilistic assessment of potential fault slip related to injection-induced earthquakes: Application to north-Central Oklahoma, USA. Geology 44 (12), 991–994. https://doi.org/10.1130/G38275.1.